IEEE Access
Multidisciplinary | Rapid Review | Open Access Journal

Received 26 May 2023, accepted 15 June 2023, date of publication 13 July 2023, date of current version 20 July 2023.

Digital Object Identifier 10.1109/ACCESS.2023.3295256

RESEARCH ARTICLE

The Effects of Channel Model and Spacing on Slanted Subarrays in Single-User MIMO mmWave Systems

EDITH GHUNNEY, (Student Member, IEEE), AND MARY ANN WEITNAUER, (Senior Member, IEEE)
School of Electrical and Computer Engineering, Georgia Institute of Technology, Atlanta, GA 30332-0250, USA
Corresponding author: Edith Ghunney (eghunney3@gatech.edu)

The work of Edith Ghunney was supported in part by the Qualcomm Fellowship, and in part by the Ghana Educational Trust Fund.

ABSTRACT Slanting of subarrays in a hybrid MIMO configuration is known to mitigate loss from directional antenna elements typical of mmWave integrated circuit arrays, under the line-of-sight (LOS) plane wave model (PWM) of propagation. This paper considers optimal slanting of subarrays under the spherical wave model (SWM) of propagation, because the SWM is known to be more appropriate than PWM for short-range LOS MIMO channels. The capacity of MIMO under the LOS SWM is known to depend on subarray spacing for non-slanted subarrays, so this paper derives the optimal spacing for slanted subarrays, which is shown to be the same as for non-slanted subarrays. The paper goes on to show that slanting only degrades hybrid MIMO capacity under the SWM model. By comparing the capacities under the PWM and SWM, the authors explain why slanting is beneficial under one model and not under the other.

INDEX TERMS Antenna radiation patterns, linear antenna arrays, millimeter wave technology, MIMO communication, phased arrays, wireless communication.

I. INTRODUCTION

5G and beyond networks aspire to connect more devices in other areas besides telephony, such as robotics and automation (applicable to industry floors, medical centers), virtual reality (applicable to gaming applications), etc. These devices and other wearables may undergo positional changes as users engage with them for optimal experience [1]. The huge bandwidth of the high-frequency millimeter wave (mmWave) and terahertz (THz) spectra for beyond 5G communications is capable of meeting the traffic demand of these new applications. Their smaller wavelength allows densely-packed antennas, which can be used to create high-gain narrow beams to limit the high inherent path loss.

Recent advancement in integrated circuits (ICs) allows the manufacturing and grouping of mmWave antennas into subarrays. The antennas in these IC subarrays necessarily have directional element patterns [2]. With directional antenna elements, the line-of-sight (LOS) path, the strongest path in mmWave, may enter the sidelobe or low-gain part of the element pattern due to the user's change in positions, thereby degrading link performance. The subarrays, together with hybrid beamforming, can create a form of multiple input multiple output (MIMO) system, where without extra bandwidth or transmit power, multiple independent data streams are transmitted or received in parallel through spatial multiplexing [3]. In [4], the authors found that tilting or "slanting" the subarrays mitigates the degradation from directional element patterns in a MIMO configuration under the plane wave model (PWM) of propagation.

The proper characterization of the propagation channel is vital to the correct calculation of link performance gain. The PWM, where the wave has the same direction of arrival and a constant amplitude across the array, gives no spatial multiplexing gain in the pure LOS channel [5]. In the strong line-of-sight (LOS) environment, if the range is short enough, the spherical wave model (SWM) is the proper

The associate editor coordinating the review of this manuscript and approving it for publication was Ravi Kumar Gangwar.

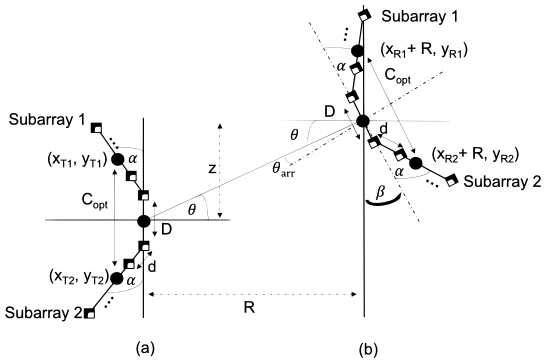

FIGURE 1. Array topology at the (a) BS and (b) UE.

propagation model and offers higher capacity through spatial multiplexing [6], [8].

For SWM, the placements of the antennas are critical for maximum spatial multiplexing gain. The optimal criterion for subarray placement in an array was derived in [9], [10], and [12]. In all these papers, the subarrays were not slanted. In [9], only the transmitter (TX) had subarrays in an analog architecture and the receiver (RX) was a linear array. The TX subarrays were all on a straight line and while the RX was rotated, the antenna elements were modeled as omnidirectional, so rotation as a compensation for directional elements was not studied. In [10] and [12], the TX and RX arrays were parallel to each other. In [4], the authors considered subarray slanting for SWM, however, the spacing of slanted subarrays was not optimized, so SWM results were not considered meaningful.

In this paper, we show that to benefit from slanting subarrays in an array, the channel model matters. For the SWM, we show that slanting subarrays does not affect the optimal inter-subarray spacing. To show this, we perform a novel analysis to derive the optimal inter-subarray spacing for array of slanted subarrays (AoSSA) for arbitrary UE orientation. To the best of our knowledge, we are the first to do this for AoSSA. We also explain why slanting subarrays under the SWM may be detrimental even with directional antenna elements, unlike in PWM. Finally, we show that the hybrid SW-PW channel model can be used to approximate the SWM when the subarrays are widely spaced.

The remainder of the paper is organized as follows. Section II provides the system model and discusses the AoSSA optimization for random UE position (orientation and location). In Section III, the design criteria for maximizing the capacity of LOS MIMO channels for AoSSA architecture are derived. Next, we discuss the AoSSA. In Section IV, the numerical evaluation of the impact of optimal AoSSA design on the capacity of the mmWave system is presented. Finally, we conclude the paper and summarize key findings in Section V.

II. SYSTEM DESCRIPTION

We assume that the base station (BS) and user equipment (UE) lie in the xy-plane as shown in Fig. 1. We consider a hybrid beamforming (HBF) architecture [13], in which the antenna elements are arranged as an array of slanted subarrays (AoSSA). We assume both the BS and the UE are equipped with 2 subarrays, each shaped as a uniform linear array (ULA), but slanted at an angle, α, as displayed in Fig. 1. We considered only 2 subarrays for 1) ease of computation and 2) the physical size constraint of user devices. To capture the effects of the rotation of the UE as a result of user activities during communication, we assume only the orientation of the UE, represented by β, is changed during communication. Parameters such as the location of the UE remain unaltered. There is no change in the orientation and location of the BS.

Each subarray contains N antenna elements, which are connected by a single RF chain to allow analog beamforming and combining at the BS and UE respectively. For a single-user multiple input, multiple output (SU-MIMO) link in the downlink HBF mode as considered in this paper, the received signal after the data streams from the BS have been first modified by the hybrid precoders and later, by the hybrid combiners at the UE, is expressed as

$$\mathbf{y} = \mathbf{U}^*\mathbf{HPs} + \mathbf{U}^*\mathbf{n}, \tag{1}$$

where $\mathbf{H} \in \mathbb{C}^{2N\times 2N}$ is the MIMO channel, $\mathbf{s} \in \mathbb{C}^{2\times 1}$ is the data symbol vector, $\mathbf{P} = \mathbf{P}_A\mathbf{P}_D \in \mathbb{C}^{2N\times 2}$ denotes the hybrid precoder where $\mathbf{P}_A$ is the analog precoder and $\mathbf{P}_D$ is the digital precoder; $\mathbf{U} = \mathbf{U}_A\mathbf{U}_D \in \mathbb{C}^{2N\times 2}$ is the hybrid combiner with $\mathbf{U}_A$ as the analog combiner and $\mathbf{U}_D$ as the digital combiner, $\mathbf{n} \sim \mathbb{CN}(\mathbf{0}, \sigma^2\mathbf{I}_{2N})$ is a complex Gaussian noise vector, and $(\cdot)^*$ denotes the Hermitian transpose.

A. CHANNEL MODEL

We assume that through a successful initial access process, a direct LOS link has been established between the BS and the UE. Hence, the direction of arrival is known. We consider only the LOS channel because it exists with high probability in mmWave [14]. Furthermore, we consider only the LOS path for our theoretical analysis, since the mmWave channel is sparse and the LOS path is by far the strongest, especially, considering that other paths are attenuated by sidelobes gains of the array patterns. The BS and UE under investigation face each other, but are separated by distance R horizontally along the x-axis, and z vertically, along the y-axis as shown in Fig. 1. The vertical spacing between the midpoints of the two subarrays in the BS (UE) is $C_T(C_R)$. $(R + x_{Ri}, y_{Ri})$ are the x- and y- coordinates of the center of the UE subarray after rotation, while (x_{Tj}, y_{Tj}) stand for the x- and y- coordinates of the center of the BS subarray. We observe that the x coordinates for the UE are relative to the UE center, while all other coordinates are absolute. The settings and parameters for the AoSSA as shown in Fig. 1 and Fig. 3 are listed in Table 1. We consider four different channel models in this paper, the hybrid SW-PW, the SWM [8], and the single-path LOS and Geometric model (GM) [11] under the PWM.

TABLE 1. Parameters for AoSSA topology.

Symbols	
α	The slant angle of a subarray relative to the y-axis
β	The orientation of the UE
R	Horizontal distance between BS and UE centers
z	Vertical distance between BS and UE centers
D	Inter-subarray distance
d	Inter-element distance
x_{T1}	x-coordinate of the midpoint of the BS subarray 1
y_{T1}	y-coordinate of the midpoint of the BS subarray 1
x_{T2}	x-coordinate of the midpoint of the BS subarray 2
y_{T2}	y-coordinate of the midpoint of the BS subarray 2
x_{R1}	x-coordinate of UE subarray 1 relative to UE center
y_{R1}	y-coordinate of the midpoint of the UE subarray 1
x_{R2}	x-coordinate of UE subarray 2 relative to UE center
y_{R2}	y-coordinate of the midpoint of the UE subarray 2
Q_{T1}	Midpoint of the BS subarray 1
Q_{T2}	Midpoint of the BS subarray 2
Q_{R1}	Midpoint of the UE subarray 1
Q_{R2}	Midpoint of the UE subarray 2
L	The length of each subarray
C_{opt}	Optimal spacing between midpoints of subarray 1 and 2
θ	Angle of departure from BS
θ_{arr}	Angle of arrival to UE considering UE orientation

1) HYBRID SW-PW MODEL

The half-wavelength spatial spacing between elements in a subarray permits the PW assumption, while the large spacing between the 2 subarrays makes the spherical-wave (SW) assumption to be appropriate [10]. This approach effectively models each subarray like a directional element in a 2×2 MIMO channel. We show in Section III that using this hybrid SW-PW configuration approximates the purely SW channel when subarrays are widely-spaced. The channel is therefore given as

$$\mathbf{H} = \mathbf{H}_s \otimes \mathbf{H}_p, \tag{2}$$

where $\mathbf{H}_s$ represents the spherical-wave channel between subarray centers, $\mathbf{H}_p$ is the plane-wave channel between subarray elements, and $\otimes$ denotes the Kronecker multiplication. $\mathbf{H}_s$ can be expressed as

$$\mathbf{H}_s = \begin{bmatrix} h_{11} & h_{12} \\ h_{21} & h_{22} \end{bmatrix}, \tag{3}$$

and $\mathbf{H}_p$ is written as

$$\mathbf{H}_p = \begin{bmatrix} \mathbf{H}_{11} & \mathbf{H}_{12} \\ \mathbf{H}_{21} & \mathbf{H}_{22} \end{bmatrix}, \tag{4}$$

where $\mathbf{H}_{i,j}$ is the channel matrix between the i-th UE subarray and the j-th BS subarray.

2) SPHERICAL WAVE MODEL

For the SW part of the Hybrid SW-PW model, assuming that the relative differences in path loss are negligible, the normalized free-space channel between one subarray at the BS and another at the UE array can be expressed mathematically as

$$h_{ij} = e^{j\frac{2\pi R_{ij}}{\lambda}}, \tag{5}$$

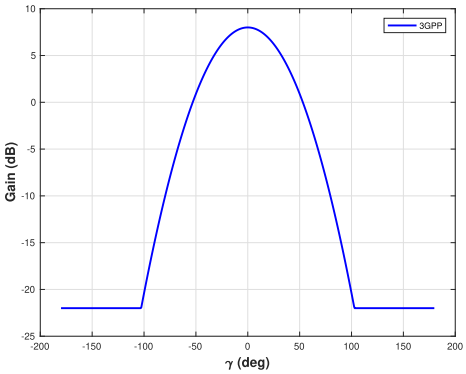

FIGURE 2. Antenna element radiation pattern for 3GPP [17].

where R_{ij} represents the distance between the centers of the j-th BS subarray and the i-th UE subarray. R_{ij} can be simplified in terms of the coordinates of the centers of the BS and the UE subarrays when $R \gg (x_{Ri} - x_{Tj})$ as

$$\begin{aligned} R_{ij} &= \sqrt{(R + x_{Ri} - x_{Tj})^2 + (y_{Ri} - y_{Tj})^2} \\ &\approx (R + x_{Ri} - x_{Tj}) + \frac{(y_{Ri} - y_{Tj})^2}{2R}. \end{aligned} \tag{6}$$

Similar to [15], the simplification in Eqn. (6) follows the second-order Taylor series approximation and will be used to decompose the channel for capacity maximization of this MIMO system in Section III-A.

3) SINGLE-PATH LINE-OF-SIGHT MODEL

Under the PW model, we first consider a single LOS path between the BS and UE. Let γ_T and γ_R denote the effective angle of departure (AoD), and effective the angle of arrival (AoA), respectively, after slanting. The channel model between the BS and UE subarrays is mathematically expressed as

$$\mathbf{H}_{i,j}(\gamma_R, \gamma_T) = \sqrt{N^2} F(\gamma_R) \mathbf{a}_{Si}(\gamma_R, 1) F(\gamma_T) \mathbf{a}^*_{Sj}(\gamma_T, -1). \tag{7}$$

where $\mathbf{a}_{Sj}(\gamma_T, -1)$ and $\mathbf{a}_{Si}(\gamma_R, 1)$ are the array responses at the j-th BS subarray and i-th UE subarray, respectively. $F(\gamma_T)$ and $F(\gamma_R)$ denote the field patterns at the j-th BS subarray and i-th UE subarray respectively, such that the boresight of the element pattern is orthogonal to the line of the linear subarray that contains the element. The field pattern, assuming identical and vertically polarized antenna elements, i.e., the polarization slant angle, $\xi = 0$, for simplicity, is given as [16] and [17]:

$$F(\gamma) = \sqrt{A_G(\gamma)} \cos(\xi) = \sqrt{A_G(\gamma)}, \tag{8}$$

where γ is the azimuth angle and $A_G(\gamma)$ is the 2D 3GPP antenna element gain as shown in Fig. 2, defined in Table 7.1-1 in [17].

As observed in Fig. 1, the UE is rotated by angle, β. This changes the direction of arrival at the UE. The Cartesian coordinates of the antenna elements of the UE are rotated by

multiplying by the matrix,

$$R_{\text{mat}} = \begin{bmatrix} \cos\beta & -\sin\beta \\ \sin\beta & \cos\beta \end{bmatrix}. \tag{9}$$

After simplification, the new AoA about the axis of symmetry of the UE, relative to the LOS between the two terminals is $\theta_{arr} = \theta - \beta$. The array response of Subarray 1 is given as

$$a_{S1}(\gamma_1, \epsilon) = \frac{1}{\sqrt{N}}[1, e^{-j\epsilon\Gamma_1}, \cdots, e^{-j\epsilon(N-1)\Gamma_1}]^T \cdot e^{j\epsilon(N-1)\Gamma_1} \cdot e^{j\Omega}, \tag{10}$$

where $\Gamma_1 = \frac{2\pi d}{\lambda}\sin(\gamma_1)$, $\gamma_1 = \alpha + \epsilon\psi$, $\psi \in \{\theta, \theta_{arr}\}$ is the AoD, θ, or the AoA, θ_{arr}, $\epsilon = 1$ for UE and $\epsilon = -1$ for BS, $d = \frac{\lambda}{2}$ represents the inter-element spacing, λ is the wavelength, and $(\cdot)^T$ denote vector transpose. The last factor in Eqn. (10) depends on the phase shift among different subarrays, expressed as

$$\Omega = \frac{2\pi}{\lambda} \cdot \frac{D}{2}\sin(\psi), \tag{11}$$

where $D = \frac{1}{2}\lambda$, but may vary in SW and Hybrid SW-PW models. The term, $e^{j\epsilon(N-1)\Gamma_1}$, is introduced to ensure $\mathbf{a}_{S1}$ has the same order as $\mathbf{a}_{S2}$.

The response of Subarray 2 is given by

$$a_{S2}(\gamma_2, \epsilon) = \frac{1}{\sqrt{N}}[1, e^{j\epsilon\Gamma_2}, \cdots, e^{j\epsilon(N-1)\Gamma_2}]^T \cdot e^{-j\Omega}, \tag{12}$$

where $\Gamma_2 = \frac{2\pi d}{\lambda}\sin(\gamma_2)$, $\gamma_2 = \alpha - \epsilon\psi$. We assume a constant ψ among all subarrays [10].

4) GEOMETRIC MODEL

The geometric mmWave channel model consists of one LOS path and $K - 1$ non LOS paths, each characterized by a decreasing average power and delay. The PWM is used for each path. The channel matrix, $\mathbf{H}_{GM}$, is represented as [11]

$$\mathbf{H}_{GM}(\gamma_R, \gamma_T) = \sqrt{\frac{N^2}{K}}\sum_{k=1}^{K} g_k F(\gamma_{R,k})\mathbf{a}(\gamma_{R,k}, 1) \cdot F(\gamma_{T,k})\mathbf{a}^*(\gamma_{T,k}, -1) \tag{13}$$

where g_k is the complex gain of the k-th path. In this paper, $K = 3$ while $g_1 \sim \mathbb{CN}(0, 1)$ and $g_{k\in\{2,3\}} \sim \mathbb{CN}(0, 0.01)$. The phase angles, ψ are independent uniform random variables over $[\frac{-\pi}{2}, \frac{-\pi}{2})$.

B. PRECODING AND COMBINING MODEL

In a partially-connected HBF structure, $\mathbf{P_A}$ is given by [13]

$$\mathbf{P}_A = diag\{\mathbf{a}_1, \mathbf{a}_2\}, \tag{14}$$

where $\mathbf{a}_i$, $i \in \{1, 2\}$, is the analog precoder of the i-th subarray, and can be expressed as

$$a_i(\gamma_{ai}, \epsilon) = \frac{1}{\sqrt{N}}[1, e^{j\epsilon\Gamma_{ai}}, \cdots, e^{j\epsilon(N-1)\Gamma_{ai}}]^T, \tag{15}$$

where $\Gamma_{ai} = \frac{2\pi d}{\lambda}\sin(\gamma_{ai})$, $\gamma_{a1} = \alpha + \epsilon\varphi_1$, and $\gamma_{a2} = \alpha - \epsilon\varphi_2$ with φ_i as the steering angle. For a perfectly aligned BS and UE, and assuming a constant steering angle among all subarrays, $\varphi_i = \psi$. On the other hand, the analog combining matrix, $\mathbf{U}_A$, is defined similarly to $\mathbf{P}_A$.

The optimal digital precoder and combiner, $\mathbf{P}_D$ and $\mathbf{U}_D$, are generated from the singular value decomposition (SVD) of the effective channel matrix, $\mathbf{H}_{\text{eff}} = \mathbf{U}_A^*\mathbf{H}\mathbf{P}_A$, as

$$\mathbf{H}_{\text{eff}} = \mathbf{W}\Lambda\mathbf{V}^*, \tag{16}$$

where $\mathbf{U}_D = \mathbf{W}$ and $\mathbf{P}_D = \mathbf{V}$.

To determine the capacity of the mmWave channel, we find the singular values, ς_i, of the 2×2 hybrid channel matrix, $\mathbf{Z}^{-\frac{1}{2}}\mathbf{U}^*\mathbf{H}\mathbf{P}$, and allocate power over the resulting parallel channels via waterfilling such that the channel capacity becomes [18]

$$S = \sum_{i}^{N_s}(\log(\mu\varsigma_i))^+, \tag{17}$$

where $\mathbf{Z} = \sigma^2\mathbf{U}^*\mathbf{U}$ is the noise covariance matrix after combining, N_s is the number of subarrays, μ is the waterfill level and x^+ is defined as $\max(x, 0)$.

To design the AoSSA such that it maximizes average capacity, we assume that θ and β follow a uniform distribution within the range of $[\frac{-\pi}{3}, \frac{\pi}{3}]$. This choice is made to accommodate the lack of control over the user's position and rotational angle within the sector. The selected range is based on the observation that beyond 60°, the antenna element pattern exhibits low gain, as illustrated in Fig. 2. Consequently, the link connection quality may deteriorate, making it more advantageous for the user to be served by another sector or base station (BS). We optimize the slant angle as

$$\alpha_{opt} = \max_{\alpha}\left(\mathbb{E}\left[S(\alpha)\right]\right). \tag{18}$$

III. OPTIMAL SUBARRAY SPACING FOR NON-ZERO α, β, θ

Assuming the SWM, the authors in [10] derive the spacing between co-linear subarrays (i.e., $\alpha = 0°$) that orthogonalizes the channel and therefore optimizes channel capacity. In this section, we prove that "slanting" the subarrays about their centers (i.e., $\alpha \neq 0°$), does not change the optimal spacing.

To optimize the capacity of the MIMO system, the maximum number of data streams transmitted should be equivalent to the number of independent single input single output (SISO) subchannels [9], [19]. The maximum capacity of the MIMO system is accomplished when the channel is orthogonal, that is, when the correlation among the array response components of the channel is driven to zero, expressed mathematically as [19]

$$\mathbf{H}_s^*\mathbf{H}_s = N\mathbf{I}_N, \tag{19}$$

where $\mathbf{I}_N$ is $N \times N$ identity matrix.

In the remainder of this section, we firstly express the orthogonality criterion in Eqn. (3) in terms of the x- and

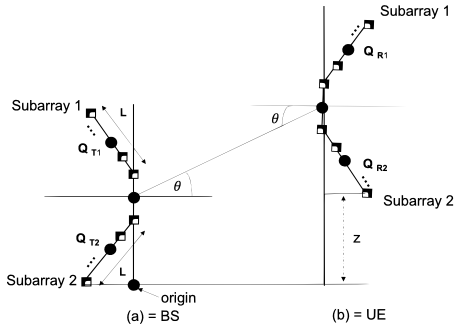

FIGURE 3. 2 × 2 AoSSA topology when $\beta = 0°$.

y-coordinates of the centers of the different subarrays. Then, secondly, we derive the coordinates under non-zero α, θ and β, and substitute these coordinates into the orthogonality criterion and simplify to express the optimal inter-subarray spacing. Finally, we show through numerical analysis that for a properly spaced subarrays, the hybrid SW-PW model could be used in lieu of the SWM.

A. THE ORTHOGONALITY CRITERION IN TERMS OF COORDINATES

Following [10], the channel matrix in Eqn. (3) can be decomposed as

$$\mathbf{H}_s = e^{j\frac{2\pi R}{\lambda}}\mathbf{H}_r\mathbf{H}_D\mathbf{H}_t, \tag{20}$$

where $\mathbf{H}_r$ and $\mathbf{H}_t$ are the diagonal matrices containing the phase shifts caused by the offsets at UE and BS respectively. Recalling that R_{ij} is the distance between the subarrays centers of the BS and UE, as stated in Eqn. (6), the diagonal members of $\{\mathbf{H}_r\}$ and $\{\mathbf{H}_t\}$ are $\{\mathbf{H}_r\}_{ii} = e^{j\frac{2\pi}{\lambda}x_{Ri}}$, and $\{\mathbf{H}_t\}_{jj} = e^{-j\frac{2\pi}{\lambda}x_{Tj}}$, respectively, and $\{\mathbf{H}_D\}_{ij} = e^{j\frac{2\pi}{\lambda}\frac{(y_{Ri}-y_{Tj})^2}{2R}}$. Because $\mathbf{H}_D$ is orthogonal just as $\mathbf{H}_S$, this orthogonality can be expressed similarly as in Eqn. (21), shown at the bottom of the page, where $d_{i,j} = (y_{Ri} - y_{Tj})^2$.

Following [19] to simplify Eqn. (21), we have

$$(y_{R1} - y_{T1})^2 - (y_{R1} - y_{T2})^2 - (y_{R2} - y_{T1})^2 + (y_{R2} - y_{T2})^2 = R\lambda. \tag{22}$$

B. OPTIMAL INTER-SUBARRAY SPACING

We first determine the positions of the midpoints of the subarrays of the BS and the UE when $\beta = 0°$, after which the new positions of UE resulting from its rotation is calculated. Let denote $L = d(N-1)\lambda$ as the length of each subarray as shown in Fig. 3. The midpoints of the two subarrays in the BS (UE), positioned at Q_{T1} and Q_{T2} (Q_{R1} and Q_{R2}) when $\beta = 0°$ are defined as

$$Q_{T1} = \begin{bmatrix} x_{T1} \\ y_{T1} \end{bmatrix} = \begin{bmatrix} -\frac{L}{2}\sin\alpha \\ C + \frac{L}{2}\cos\alpha \end{bmatrix},$$
$$Q_{T2} = \begin{bmatrix} x_{T2} \\ y_{T2} \end{bmatrix} = \begin{bmatrix} -\frac{L}{2}\sin\alpha \\ \frac{L}{2}\cos\alpha \end{bmatrix}, \tag{23}$$
$$Q_{R1} = \left[R + \frac{L}{2}\sin\alpha, \left(z + C + \frac{L}{2}\cos\alpha\right)\right]^T,$$
$$Q_{R2} = \left[R + \frac{L}{2}\sin\alpha, \left(z + \frac{L}{2}\cos\alpha\right)\right]^T. \tag{24}$$

z is the same as the distance between last antenna element in Subarray 2 of the BS and UE as depicted in Fig. 3. There is a direct proportionality between z and θ, where $\theta = \arctan(\frac{z}{R})$.

Now, we will find the position of UE when $\beta \neq 0°$. After UE rotation about the center of UE, β is no longer 0°, and the positions of the subarrays midpoints of the UE are changed. Using R_{mat} from Eqn. (9), the new coordinates can be determined as

$$\mathrm{Q}_{new} = R_{\text{mat}} \times ([Q_{Ri}] - [Q_{UE}]) + [Q_{UE}] \tag{25}$$

where $Q_{UE} = [R, z + \frac{C}{2} + \frac{L}{2}\cos\alpha]$ is the center of the UE. From Eqn. (25), the UE midpoint coordinates after rotation become

$$\begin{bmatrix} x_{R1} + R \\ y_{R1} \end{bmatrix} = \begin{bmatrix} \frac{L}{2}\sin\alpha\cos\beta - \frac{C}{2}\sin\beta + R \\ \frac{L}{2}\sin\alpha\sin\beta + \frac{C}{2}\cos\beta + z + \frac{C}{2} + \frac{L}{2}\cos\alpha \end{bmatrix},$$

$$\begin{bmatrix} x_{R2} + R \\ y_{R2} \end{bmatrix} = \begin{bmatrix} \frac{L}{2}\sin\alpha\cos\beta + \frac{C}{2}\sin\beta + R \\ \frac{L}{2}\sin\alpha\sin\beta - \frac{C}{2}\cos\beta + z + \frac{C}{2} + \frac{L}{2}\cos\alpha \end{bmatrix}. \tag{26}$$

By substituting the $y-$coordinates of Eqn. (23) and Eqn. (26) for the midpoints of the BS and UE respectively, the maximum capacity criterion of Eqn. (19) becomes

$$C_{opt} = \sqrt{\frac{R\lambda}{2\cos\beta}}. \tag{27}$$

The derived C_{opt} is the same as the optimal inter-subarray spacing found in [9] where $\alpha = 0°$ at the BS (array-of-subarrays) and the UE (array-of-elements) for $\beta \neq 0°$. When $\beta = 0°$, C_{opt} in Eqn. (27) is the same as the result in [10] (BS and UE are array-of-subarrays) and [12] (BS and UE are array-of-elements). The above equation shows that, the optimal inter-subarray spacing, C_{opt}, is independent of the slant angle, α, and the BS angle of departure, θ.

We observe that it is impractical to modify C_{opt} as the user rotates, i.e., as β changes. Therefore, some fixed value of β, which we denote as β_{25}, must be selected in Eqn. (27); this selected value would be used by IC manufacturer. In Section IV-C, optimization of β_{25} is considered.

$$\mathbf{H}_D^*\mathbf{H}_D = N\mathbf{I}_N \begin{bmatrix} 2 & e^{j\frac{\pi}{R\lambda}(d_{1,1}-d_{1,2})} + e^{j\frac{\pi}{R\lambda}(d_{2,1}-d_{2,2})} \\ e^{j\frac{\pi}{R\lambda}(d_{1,2}-d_{1,1})} + e^{j\frac{\pi}{R\lambda}(d_{2,2}-d_{2,1})} & 2 \end{bmatrix} = 2\begin{bmatrix} 1 & 0 \\ 0 & 1 \end{bmatrix} \tag{21}$$

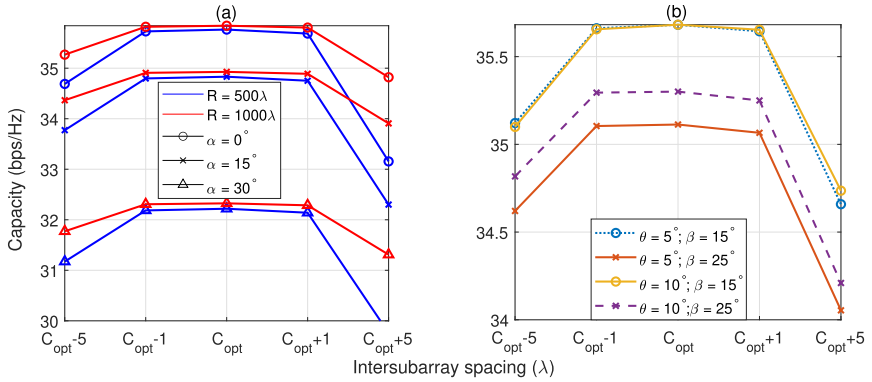

FIGURE 4. Capacity vs different inter-subarray spacings for (a) different R and α when $\theta = 0°$, $\beta = 0°$, and (b) different β and θ when $\alpha = 0°$, $R = 1000\lambda$. We assume $N = 8$, SNR = 20 dB and C_{opt} is the optimal inter-subarray spacing.

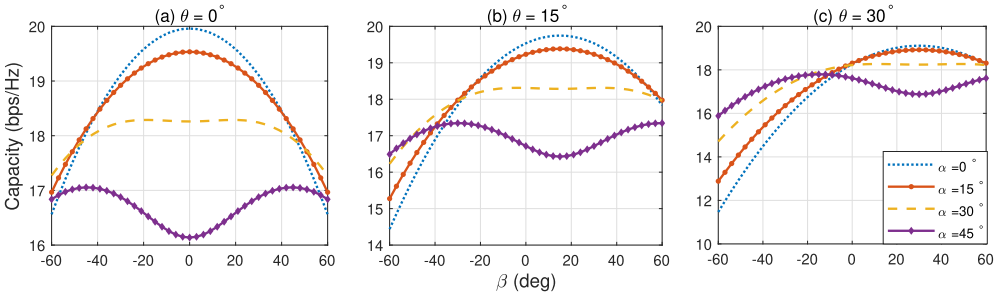

FIGURE 5. Capacity of single-path LOS PWM computed over β range of $[\frac{-\pi}{3}, \frac{\pi}{3}]$ for different α when (a) $\theta = 0°$, (b) $\theta = 15°$ and (c) $\theta = 30°$, using 3GPP antenna elements, $N = 8$, $\beta_{25} = 0°$ and SNR = 20 dB.

IV. NUMERICAL EVALUATION

In this section, we use Monte Carlo simulation to A) validate the optimal inter-subarray spacing derived in the previous section, B) investigate how capacity depends on propagation model, user rotation (β), and subarray slant angle (α), and demonstrate that the hybrid SW-PW model closely approximates the SW model regardless of these parameters, C) find an optimum value of β_{25}, and D) determine the optimum slant angle for 120° sector in terms of average capacity.

The following parameters are used in the Monte Carlo simulations, unless otherwise stated. Each subarray in the AoSSA at both the BS and UE contains $N = 8$, for a total number of 16 antenna elements per terminal. We apply the 3GPP antenna model to compute the antenna element field patterns as in Eqn. (8) [16], [17]. We assume SNR = 20 dB and a field of view (FoV) of $[\frac{-\pi}{3}, \frac{\pi}{3}]$. For the SWM evaluation, we assume BS-UE distance of 1000λ unless otherwise stated.

A. VALIDATION OF OPTIMAL SUBARRAY SPACING

We validate the derivation of optimal inter-subarray spacing for AoSSA in Eqn. (27). Fig. 4 (a) plots the capacity vs inter-subarray spacing for different slant angle (α) and BS-UE distances (R), when AoD, $\psi = 0°$, and $\beta = 0°$. It can be observed that capacity is somewhat insensitive to subarray spacing over the range $C_{opt} \pm 1$, however it is maximized by C_{opt} regardless of the R and α considered.

Fig. 4 (b) plots the capacity vs the inter-subarray spacing for different ψ and β. Again, we observe insensitivity over a range, but the C_{opt} as derived in Eqn. (27) maximizes the capacity.

B. EFFECTS OF PROPAGATION MODEL AND SLANT ANGLE ON CAPACITY, FOR DIFFERENT USER ROTATIONS

In this section, we seek to understand why the capacity response to subarray slant angle and user rotation is different for the PW and SW propagation models. We also show that the Hybrid SW-PW model is a good approximation for the SW model.

Fig. 5 shows the capacity, against β for different α, using the single-path LOS PW channel model. Figures (a), (b) and (c) represent the capacity when $\theta = 0°$, $\theta = 15°$, and $\theta = 30°$, respectively.

The PWM results in Fig. 5 show that the β that yields the highest capacity depends on α. For $\alpha = 0°$ and 15°, the location of the single peak is at the β value that corresponds to θ, but for the higher α values, symmetric peaks occur at $\beta = \theta \pm \alpha$. Since under the PWM, there is no spatial multiplexing gain due to rank limitation [10], the performance is dominated by the BS and UE pair of subarrays that enjoy the highest gain in the element pattern. When $\beta = \theta \pm \alpha$, one subarray from the BS and one from the UE face each other.

We see in Fig. 5 that as the θ grows, the curves for different α are less separated. For example, for $\theta = 0°$ (Fig. 5a),

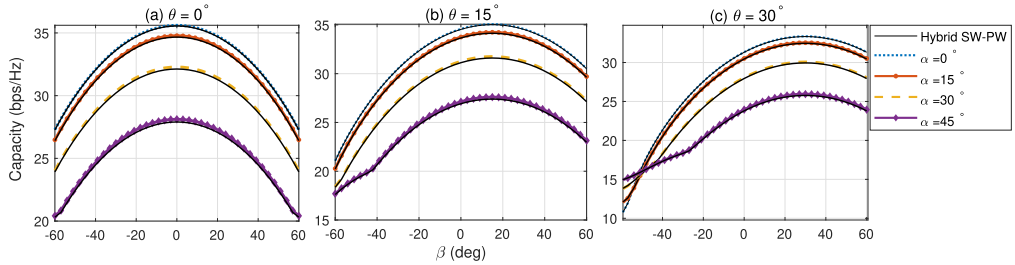

FIGURE 6. Comparison of capacity for hybrid SW-PW (black curves) and SWM (non-black colored curves) computed over β range of $[\frac{-\pi}{3}, \frac{\pi}{3}]$ for different α with (a) $\theta = 0°$, (b) $\theta = 15°$ and (c) $\theta = 30°$, using 3GPP antenna elements, $N = 8$, $\beta_{25} = 0°$ and SNR = 20 dB.

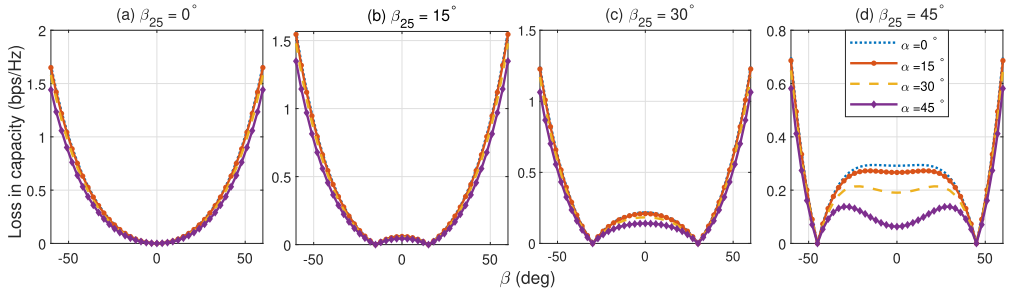

FIGURE 7. Loss in capacity when subarray spacing is computed sub-optimally as stated in Eqn. (27) for (a) $\beta_{25} = 0°$, (b) $\beta_{25} = 15°$, (c) $\beta_{25} = 30°$ and (d) $\beta_{25} = 45°$ over β range of $[\frac{-\pi}{3}, \frac{\pi}{3}]$ for different α, using 3GPP antenna elements in the hybrid SW-PW model, $\theta = 0°$, $N = 8$ and SNR = 20 dB.

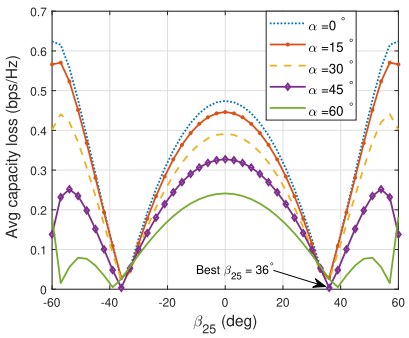

FIGURE 8. Average loss in capacity vs β_{25}, averaged over $[\frac{-\pi}{3}, \frac{\pi}{3}]$ FoV and $[\frac{-\pi}{3}, \frac{\pi}{3}]$ range of UE rotation for different α using 3GPP antenna elements in the with hybrid SW-PW model, $N = 8$ and SNR = 20 dB.

the $\alpha = 45°$ curve is obviously lower than the $\alpha = 0°$ curve. However, for $\theta = 30°$ (Fig. 5c), this is no longer true. Anticipating that in IV-D, we will be averaging over θ and β, we can see in Fig. 5 (c) that the average of the curve for $\alpha = 30°$ looks like it will be higher than the average of $\alpha = 0°$. In other words, it would appear that slanting the subarrays is better on the average for some relative BS and US positions (i.e., some θ values). These observations will be justified in Section IV-D.

Fig. 6 is similar to Fig. 5 in terms of axes and parameters, with the primary difference being the propagation models. While Fig. 5 assumed the PW model, Fig. 6 considers both the SW and the Hybrid SW-PW models when C_{opt} is computed with $\beta_{25} = 0°$. The first observation about Fig. 6 is that there is a very little difference between the curves for the SW and Hybrid SW-PW models. To our knowledge, these two models have not been directly compared before. To demonstrate that arrays with widely spaced antennas can achieve full rank in strong LOS channels, [8] and [12] used the SWM to describe the MIMO channel of array-of-elements and array-of-subarrays respectively. On the other hand, the authors in [10] used hybrid SW-PW to model the channel for array-of-subarrays. Fig. 6 shows that the Hybrid SW-PW model is a very good approximation to the SW model over a large variety of relative configurations. Specifically, the minimum and maximum absolute differences between the capacity of the SWM and Hybrid SW-PW over the whole range of β shown are 0.05 bits/s/Hz and 0.2 bits/s/Hz for $\alpha = 0°$ and $\alpha = 45°$ respectively, and averages $\sim$ 0.14 bits/s/Hz when averaged across the slant angles. These small differences show that the hybrid SW-PW model and the purely SWM can be used interchangeably when subarray element spacing is $\frac{\lambda}{2}$.

A second observation from Fig. 6 is that the capacities are all much higher than those of Fig. 5. This can be attributed to the spatial multiplexing gain from properly spaced subarrays which is already known from [8], [10], and [12]. A more interesting observation is that, unlike in Fig. 5, the increase in θ does not cause the curves for different α to grow closer together and does not cause multiple peaks. It is clear that there is no non-zero α for which the average over β will be highest.

C. THE BEST β_{25} FOR CAPACITY LOSS REDUCTION

Eqn. (27) shows that the optimal spacing between subarrays depends on the rotation angle (β) of the UE, which

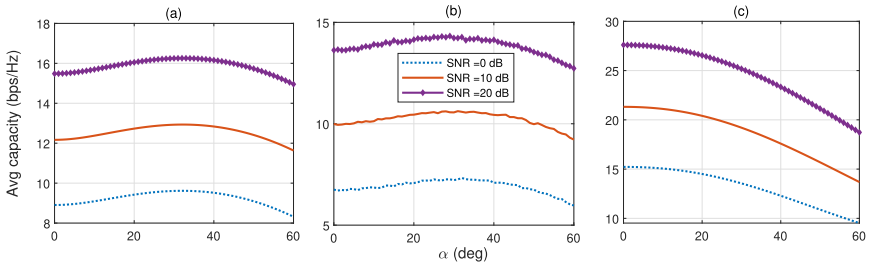

FIGURE 9. Average capacity vs α, averaged over $[\frac{-\pi}{3}, \frac{\pi}{3}]$ FoV and $[\frac{-\pi}{3}, \frac{\pi}{3}]$ range of UE rotation, for different SNRs using (a) single-path LOS, (b) GM and (c) hybrid SW-PW model when $N = 8$ and $\beta_{25} = 36°$.

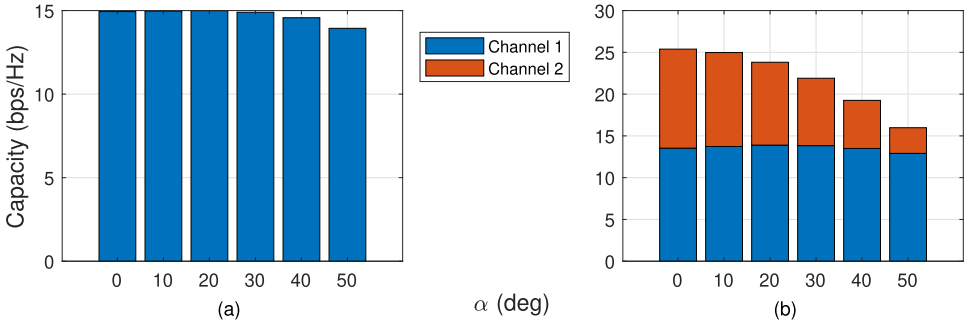

FIGURE 10. Capacity vs slant angles with (a) single-path LOS PWM and (b) hybrid SW-PW model using 3GPP antenna elements, $N = 8$, SNR = 10 dB, $\beta_{25} = 36°$ and $\theta = 30°$.

can change constantly as a user moves. Since changing the spacing of the subarrays when the UE rotates is not practical, we experiment with different β_{25} values to determine the best β_{25}, i.e., the β_{25} which gives the least loss in capacity as the actual β varies. Fig. 7 shows the penalty in capacity as a function of β for different α for (a) $\beta_{25} = 0°$, (b) $\beta_{25} = 15°$, (c) $\beta_{25} = 30°$ and (d) $\beta_{25} = 45°$ when $\theta = 0°$. We observe that the worst-case loss in capacity shrinks as β_{25} grows. The worst case loss is reduced by more than half by increasing β_{25} from 0° to 45°, as seen when Fig. 7 (a) is compared with Fig. 7 (d).

Next, we attempt to optimize β in terms of average loss in capacity. Fig. 8, shows the average loss in capacity as a function of β_{25}, for different α, when both θ and β are averaged over for the range $[\frac{-\pi}{3}, \frac{\pi}{3}]$. It is obvious that on average, $35 \leq| \beta_{25} |\leq 40$ provides the lowest loss in capacity regardless of the slant angle, α. This implies that to get the best capacity under user rotation, the designer should use $35 \leq| \beta_{25} |\leq 40$ to get the best suboptimal inter-subarray spacing in AoSSA.

D. OPTIMUM SLANT ANGLE

In Fig. 9, we plot the average capacity, where the average is taken over every angle, θ, in the FoV, and every UE rotation, β, in the range, $[\frac{-\pi}{3}, \frac{\pi}{3}]$, across different α. The single-path LOS, the GM, and the SWM are displayed in Fig. 9 (a), (b), and (c) respectively. For SWM, we use the best $\beta_{25} = 36°$ as indicated in Fig. 8. In Fig. 9 (a), we observe that slanting the subarray at an angle of 32° optimizes the average capacity for all three SNRs considered, leading to an increase of about 1 bps/Hz, compared to the no-slant case, $\alpha = 0°$. The curves for the GM in Fig. 9 (b) are also optimized by approximately the same slant angle angle of 32°. However, for the SWM, slanting only reduces the average capacity, in spite of the best fixed subarray spacing, β_{25}, being used. Fig. 9 is similar to Fig. 5 (d) in [4], however, the best fixed subarray spacing was not used in [4].

To gain more insight into why the SWM case does not benefit from slanting, we consider the individual terms in Eqn. (17) as a function of α, for the special but representative case of $\beta = 36°$ and $\theta = 30°$ shown in Fig. 10. Fig. 10 (a), which represents the PWM, has one spatial channel (rank=1). On the other hand, the hybrid SW-PW model has two spatial channels (rank=2), where Channel 1 and Channel 2 are denoted by the stacked blue and orange bars respectively. We observe that the trend in Fig. 10 (a) is similar to that of Channel 1 in Fig. 10 (b) with only a small change in capacity as α increases. However, in Channel 2, there is a drastic drop in capacity (∼75%) between $\alpha = 0°$ and $\alpha = 50°$. For $\beta = 36°$ and $\theta = 30°$, this happens in such an orientation because one subarray of the UE and one subarray of the BS face far away from each other, resulting in very low element pattern gains on the LOS path between those two subarrays, making the channel almost rank 1. Strictly speaking, it is still a rank 2 MIMO channel, but at the power levels considered, the second mode gets very little power allocated to it. This diminishing of the magnitude of the second term in Eqn. (17) with α was also observed for β values of 0° and 30°. Therefore, we conclude that slanting the subarrays diminishes the second MIMO mode so significantly that the overall

capacity does not benefit from slanting when the SW model is in force.

V. CONCLUSION AND FUTURE WORK

In this paper, we first we derived the optimal spacing under SWM and when both ends of the MIMO link have slanted arrays, as a function of UE rotation, which showed the optimal spacing of subarrays under the SWM model is independent of slant angle. We identified the best β to help IC designers choose practical inter-subarray spacing for AoSSA considering user rotation. On the average, $\alpha_{opt} = 32°$ is the best choice in PWM for the 3GPP element pattern, but slanting subarrays hurts performance in SWM. Thus, we recommend slanting for longer range links where the PW model is appropriate, but no slanting for shorter links where the SW model is appropriate. We also explained why slanting of subarray is ineffective in the SWM compared to the PWM. Finally, we showed that the hybrid SW-PW model and the purely SWM can be used interchangeably when subarrays are widely separated.

Suggestions for future work include expanding this study beyond two subarrays, exploring the utilization of planar arrays as the subarrays, and investigating the applicability of this architecture for multi-user multiple-input multiple-output (MU MIMO) scenarios. In MU MIMO, the selection of subarrays with the highest spectral efficiency could be employed to serve users optimally.

REFERENCES

[1] F. Pallavicini, A. Pepe, and M. E. Minissi, "Gaming in virtual reality: What changes in terms of usability, emotional response and sense of presence compared to non-immersive video games?" *Simul. Gaming*, vol. 50, no. 2, pp. 136–159, Apr. 2019.
[2] B. Sadhu et al., "A 28-GHz 32-element TRX phased-array IC with concurrent dual-polarized operation and orthogonal phase and gain control for 5G communications," *IEEE J. Solid-State Circuits*, vol. 52, no. 12, pp. 3373–3391, Dec. 2017.
[3] D. Gesbert, M. Shafi, D.-S. Shiu, P. J. Smith, and A. Naguib, "From theory to practice: An overview of MIMO space-time coded wireless systems," *IEEE J. Sel. Areas Commun.*, vol. 21, no. 3, pp. 281–302, Apr. 2003.
[4] E. Ghunney and M. A. Weitnauer, "Slanting mmWave subarrays in the hybrid architecture to compensate for directional antenna elements," in *Proc. IEEE Global Commun. Conf.*, Rio de Janeiro, Brazil, Dec. 2022, pp. 5426–5431, doi: 10.1109/GLOBECOM48099.2022.10001433.
[5] K. Sakaguchi, "MIMO channel capacity in an indoor line-of-sight (LOS) environment," *IEICE Trans. Commun.*, vol. 88, no. 7, pp. 3010–3019, Jul. 2005.
[6] P. F. Driessen and G. J. Foschini, "On the capacity formula for multiple input-multiple output wireless channels: A geometric interpretation," *IEEE Trans. Commun.*, vol. 47, no. 2, pp. 173–176, Feb. 1999.
[7] C. Hofmann, A. Knopp, and B. Lankl, "Indoor LoS MIMO channel measurements with a focus on antenna array design," in *Proc. IEEE Glob. Telecommun. Conf.*, Dec. 2010, pp. 1–5.
[8] J.-S. Jiang and M. A. Ingram, "Spherical-wave model for short-range MIMO," *IEEE Trans. Commun.*, vol. 53, no. 9, pp. 1534–1541, Sep. 2005.
[9] C. Xue, S. He, F. Ou, M. Wei, Y. Huang, and L. Yang, "Asymmetric subarray structure design for mmWave LoS MIMO communication systems," in *Proc. IEEE/CIC Int. Conf. Commun. China (ICCC)*, Jul. 2016, pp. 1–6, doi: 10.1109/ICCChina.2016.7636894.
[10] X. Song, W. Rave, N. Babu, S. Majhi, and G. Fettweis, "Two-level spatial multiplexing using hybrid beamforming for millimeter-wave backhaul," *IEEE Trans. Wireless Commun.*, vol. 17, no. 7, pp. 4830–4844, Jul. 2018.
[11] A. Alkhateeb, O. E. Ayach, G. Leus, and R. W. Heath Jr., "Channel estimation and hybrid precoding for millimeter wave cellular systems," *IEEE J. Sel. Topics Signal Process.*, vol. 8, no. 5, pp. 831–846, Oct. 2014.
[12] E. Torkildson, U. Madhow, and M. Rodwell, "Indoor millimeter wave MIMO: Feasibility and performance," *IEEE Trans. Wireless Commun.*, vol. 10, no. 12, pp. 4150–4160, Dec. 2011.
[13] S. He, C. Qi, Y. Wu, and Y. Huang, "Energy-efficient transceiver design for hybrid sub-array architecture MIMO systems," *IEEE Access*, vol. 4, pp. 9895–9905, 2016.
[14] Y. Azar, G. N. Wong, K. Wang, R. Mayzus, J. K. Schulz, H. Zhao, F. Gutierrez, D. Hwang, and T. S. Rappapor, "28 GHz propagation measurements for outdoor cellular communications using steerable beam antennas in New York city," in *Proc. IEEE Int. Commun. Conf.*, Mar. 2013, pp. 5143–5147.
[15] P. Larsson, "Lattice array receiver and sender for spatially orthonormal MIMO communication," in *Proc. IEEE 61st Veh. Technol. Conf.*, May 2005, pp. 192–196, doi: 10.1109/VETECS.2005.1543276.
[16] *Technical Specification Group Radio Access Network; Study on Channel Model for Frequency Spectrum Above 6 GHz*, 3GPP, document TR 38.900, 2016.
[17] *Technical Specification Group Radio Access Network; Study on 3D Channel Model for LTE*, 3GPP, document TR 36.873, 2017.
[18] A. Goldsmith, S. A. Jafar, N. Jindal, and S. Vishwanath, "Capacity limits of MIMO channels," *IEEE J. Sel. Areas Commun.*, vol. 21, no. 5, pp. 684–702, Jun. 2003.
[19] I. Sarris and A. R. Nix, "Design and performance assessment of high-capacity MIMO architectures in the presence of a line-of-sight component," *IEEE Trans. Veh. Technol.*, vol. 56, no. 4, pp. 2194–2202, Jul. 2007, doi: 10.1109/TVT.2007.897240.
[20] L. Zheng and D. N. C. Tse, "Diversity and multiplexing: A fundamental tradeoff in multiple-antenna channels," *IEEE Trans. Inf. Theory*, vol. 49, no. 5, pp. 1073–1096, May 2003.

EDITH GHUNNEY (Student Member, IEEE) received the B.S. degree in telecommunications engineering from the Kwame Nkrumah University of Science and Technology (KNUST), Kumasi, Ghana, in 2015. She is currently pursuing the Ph.D. degree in electrical and computer engineering with the Georgia Institute of Technology, Atlanta, GA, USA.

From 2015 to 2016, she was a Research Assistant with the Telecommunications Engineering Department, KNUST. Her industry experience includes a internship position with Vodafone, Ghana, and U.S. Cellular. Her research interests include mmWave communication, artificial intelligence, and emergency response and recovery.

Ms. Ghunney was a recipient of the 2018 Facebook (Meta) Emerging Scholar Award, the 2019 Google Conference and Travel Scholarship, the 2022 Qualcomm Fellowship, and the Ghana Education TrustFund (GETFund) Scholarship.

MARY ANN WEITNAUER (Senior Member, IEEE) received the B.S. and Ph.D. degrees from the School of Electrical and Computer Engineering (ECE), Georgia Institute of Technology, in 1983 and 1989, respectively, where she joined as an Assistant Professor in 1989. She was a Visiting Professor with Aalborg University, Aalborg, Denmark, from summer of 2006 to 2008, and with Idaho National Labs, in 2010. She leads the Electronic ARTrium Laboratory, which she established, in 2021. She held the Georgia Tech ADVANCE Professorship with the College of Engineering, from 2006 to 2012, where she was responsible for initiatives to help the female faculty of the college to succeed. She is currently a Professor with the School of Electrical and Computer Engineering (ECE), Georgia Institute of Technology. Her research interests include MIMO wireless communications and sensor-driven, marker-less, interactive, and immersive digital art. She leads the Electronic ARTrium Laboratory, which she established, in 2021.

She was the Senior Associate Chair of the School of Electrical and Computer Engineering, from 2016 to 2021, where she was responsible for academic operations. She was an Associate Editor of the IEEE TRANSACTIONS ON MOBILE COMPUTING, from 2009 to 2012.